Low dimensionalization of magnetic ordering in Sr_2VO_4 by hydride ion substitution

Joonho Bang,[1] Satoru Matsuishi,[2] Sachiko Maki,[2] Jun-ichi Yamaura,[2] Masatoshi Hiraishi,[3] Soshi Takeshita,[3] Ichihiro Yamauchi,[3] Kenji M. Kojima,[3] and Hideo Hosono[1,2,4,*]

[1]*Materials and Structures Laboratory, Tokyo Institute of Technology, Yokohama 226-8503, Japan*

[2]*Materials Research Center for Element Strategy, Tokyo Institute of Technology, Yokohama 226-8503, Japan*

[3]*Institute of Materials Structure Science, High Energy Accelerator Research Organization (KEK), Tsukuba, Ibaraki 305-0801, Japan*

[4]*Frontier Research Center, Tokyo Institute of Technology, Yokohama 226-8503, Japan*

(Received 28 January 2015; revised manuscript received 11 June 2015; published 11 August 2015)

Substitution of an oxygen anion with a hydrogen anion induced the low dimensionalization of magnetic ordering in a transition metal oxide Sr_2VO_4. Upon increasing x up to ~1 in $Sr_2VO_{4-x}H_x$, the hydride ions were ordered linearly, and the magnetic susceptibility was simultaneously suppressed. It was found that this suppression was attributed to the formation of a quasi-one-dimensional antiferromagnetic spin chain, maintaining that each of the vanadium cations is two-dimensionally bridged by hydride and oxide ions. Density functional theory calculations demonstrate that the quasi-one-dimensional property is caused by much enhanced anisotropic exchange couplings ($J_1/J_2 \sim 6$) originating from the absence of π bonding between H 1s and V 3d orbitals. Utilizing a hydride ion that has an ionic radius similar to an oxygen anion and only one energetically available orbital of 1s is a different approach to realization of magnetic low dimensionalization in 3d early transition metal oxides.

DOI: 10.1103/PhysRevB.92.064414 PACS number(s): 75.10.Pq, 75.30.−m, 75.30.Gw, 75.30.Et

I. INTRODUCTION

Hydrogen is the most abundant element in the universe and it is also the simplest bipolar element. Recently, the hydride ion (H^-) has been of great interest in the solid-state community because of its unique electronic structure. Hydrogen has only one energetically available atomic orbital (the spherical 1s orbital), which is totally different from conventional anions such as oxygen and the halogens. It is expected that this unique electronic nature would provide the opportunity to realize interesting physical properties in the compounds. In particular, we think utilization of hydride ion in transition metal (*TM*) oxides would be promising for the emergence of unique properties because the ionic radius of the hydride ion is similar to that of the oxide ion and there exists a distinct diversity in the chemical bonding by tuning the d electron count and available anion orbitals. Several *TM* oxyhydride compounds have been studied [1–7], but the role of the hydride ion in the physical properties is still veiled.

In general, *TM* oxyhydrides have a perovskite structure with a 3d *TM* cation. In the case of simple perovskite-type oxyhydrides such as $ATiO_{3-x}H_x$ (A = Ca, Sr, and Ba) [4,5], oxygen and hydrogen are statistically located in equivalent anion sites. In contrast, in layered perovskite-type compounds such as $LaSrCoO_3H_{0.72}$ [1], there are nonequivalent anion sites and hydrogen and oxygen are isolated by different anion sites. In the previous paper [6], we reported the synthesis of compositionally tunable vanadium oxyhydrides, $Sr_2VO_{4-x}H_x$, without accompanying the formation of considerable anion vacancies. We found hydrogen ordering and the corresponding structural transition with various O^{2-}/H^- contents using a combination of neutron diffraction, synchrotron x-ray diffraction, thermal desorption spectroscopy, and first-principles density functional theory (DFT) calculations. In the low hydrogen substitution region ($x < 0.25$), hydrogen anions statistically occupy both anion sites in the V-O and Sr-O planes. With higher hydrogen substitution ($x > 0.25$), hydrogen anions tend to occupy the anion sites in the V-O planes. As more hydrogen is incorporated, the degree of anion order increases and finally most of the hydrogen anions are located between the square planes of the oxide ions with a crystallographic phase transition [see crystal structure in Fig. 3(a)]. Subsequently, Romero *et al.* reported a checkerboard-type antiferromagnetic ground state of Sr_2VO_3H with a Néel temperature (T_N) of ~170 K by a low-temperature neutron study and muon spin rotation measurements [7].

Partial substitution of the oxide ion sites with hydride ions decreases the occupancy in the π-antibonding (π^*) molecular orbital with formation of strong σ bonds, which decreases the total energy of the crystal system. The extent of stabilization is more effective when hydrogen is located in the metal-oxide plane whose anion site is coordinated to two *TM* cations. Therefore, hydride ions are gradually ordered to the V-O planes with increasing hydrogen amount. Moreover, the *trans* configuration of the hydride ion is stereochemically more stable than the *cis* configuration, so hydride ions are finally located between the square planes of oxide ions. This anion-ordered crystal structure is also found in the Co-based layered oxyhydride $LaSrCoO_3H_{0.72}$ [1]. This type of hydrogen ordering forms two types of interaction pathways, *TM*-O-*TM* and *TM*-H-*TM*. Therefore, strong anisotropic behavior should be expected because of the different bonding nature between *TM* and O^{2-}/H^-.

In *TM* oxyhydrides, *TM* cations are octahedrally coordinated to both oxide ions with a $2p^6$ electronic configuration, and hydride ions with a $1s^2$ configuration. Although the O 2p orbitals participate in both σ bonding with *TM* $d_{x^2-y^2}$ and d_{z^2} orbitals and π bonding with *TM* d_{xy}, d_{yz}, and d_{xz} orbitals, the H 1s orbital only participates in σ bonding with *TM* $d_{x^2-y^2}$ and d_{z^2} orbitals. The contribution of hydrogen to π bonding is negligible because the H 2p level is located ~10 eV above the H 1s level. For a localized spin system such as a Mott-Hubbard insulator, there is no significant overlap between *TM* cations.

*hosono@msl.titech.ac.jp

Therefore, the role of the "bridging" anion is important because the dominant part of the exchange interaction is a superexchange interaction through the intervening anion. In the case of the superexchange interaction, one key issue is the symmetry relation between the occupied d orbitals of the cation and the p or s orbitals of the anion [8]. From this point of view, a strong anisotropic exchange interaction can be achieved by the different orbital nature of the bridging anions, and low dimensionality may be expected in anion-ordered oxyhydrides. Here, we demonstrate the role of the hydride ion in the physical dimensionality of *TM* compounds by showing the quasi-one-dimensional (1D) antiferromagnetic (AFM) spin chain in the three-dimensional crystal structure of $Sr_2VO_{4-x}H_x$ with $x \sim 1$. Although understanding low dimensionality in the *TM* oxide system is crucial for emerging unique physical properties ranging from high-temperature superconductors to spintronic devices, the magnetic dimensionality is generally restricted by the crystal structure [9–12], because the exchange interaction strongly depends on the geometrical parameters such as interatomic separation between magnetic ions. For this reason, utilization of hydride ions for emerging an anisotropic exchange interaction in three-dimensional crystal structures provides an idea for tuning the physical dimensionality in *TM* oxide systems.

II. EXPERIMENT

Polycrystalline samples of $Sr_2VO_{4-x}H_x$ were synthesized by high-pressure solid-state reaction [6]. The electrical resistivity and the specific heat capacity were measured using a physical property measurement system (Quantum Design Inc., USA). The magnetic susceptibility was characterized using a magnetic property measurement system (Quantum Design Inc., USA). Muon spin rotation (μSR) measurements were performed at the M20 channel at TRIUMF (Canada). Synchrotron radiation experiments were performed at BL-8A in KEK-PF (Proposal No. 2013S2-002). DFT calculations were performed using the experimental crystallographic parameters within the full-potential linearized augmented-plane-wave (LAPW) method implemented in the WIEN2K package [13,14]. The general gradient approximation [15] (GGA) was used for the exchange-correlation potential with on-site repulsion (U). The product of the muffin-tin radius (R_{MT}) and the largest wave number of the basis set (K_{max}) was fixed at 6.0, and the charge density was Fourier expanded up to $G_{max} = 20\,\text{Bohr}^{-1}$. We employed the following R_{MT} values : $R_{MT\text{-}Sr} = 2.34\,\text{Bohr}$, $R_{MT\text{-}V} = 1.92\,\text{Bohr}$, $R_{MT-O} = 1.73\,\text{Bohr}$, and $R_{MT\text{-}H} = 1.21\,\text{Bohr}$. Self-consistency was carried out for four types of spin-ordered states using a $2a \times 2b \times c$ supercell containing 56 atoms, and a $6 \times 6 \times 12$ k-point mesh was used. The energy convergence was set to 10^{-6} Ry for self-consistency. To calculate the hopping integral between V and O, and V and H orbitals, the maximally localized Wannier functions (MLWFs) for V $3d$, O $2p$, and H $1s$ orbitals were constructed (see Table S1 in the Supplemental Material [16]) using the WANNIER90 [17] and WIEN2WANNIER [18] codes.

III. RESULTS AND DISCUSSION

Figures 1(a) and 1(b) show the temperature-dependent magnetic susceptibility of $Sr_2VO_{4-x}H_x$. For $x = 0.04$, the $\chi(T)$ curve shows two anomalous points, at 100 and 10 K [Fig. 1(a), inset], which are known as the orbital ordering [19] and magnetic transition [20] (AFM ordering), respectively. When H^- is introduced into the oxygen site, the magnetic susceptibility in the range 2–300 K increases with increasing x until $x \sim 0.3$, and then dramatically decreases until $x = 1.00$. The $\chi(T)$ curve of $x = 1.00$ (Sr_2VO_3H, $3d^2$) shows the lowest magnetic susceptibility throughout the whole temperature range. We found a small anomalous point at around 160 K, which is close to T_N (~170 K) [7], and magnetic suppression above 160 K with a large deviation from Curie-Weiss behavior [Fig. 1(b), inset]. There is no significant difference between the zero-field cooling (ZFC) and field cooling (FC) curves. This magnetic behavior of Sr_2VO_3H is different from that reported in a previous study [7]; i.e., it shows the lack of both a signature related to AFM ordering and magnetic suppression above 160 K in the $\chi(T)$ curve with a considerable difference between the ZFC and FC curves. Considering that the magnetic susceptibility for $x = 1.00$ is about an order of magnitude smaller than the results in the previous study in the whole temperature range, these differences appear to arise from contamination of the secondary phases or a small deviation of the hydrogen content because of the different synthetic route. Figure 1(c) shows the temperature-dependent electrical resistivity of polycrystalline $Sr_2VO_{4-x}H_x$. All of the samples show a positive slope with a linear relationship between $\log \rho$ and $1/T$. Assuming that the electrical conductivity is caused by band electrons thermally excited across the band gap, the gap size is estimated to be 109 meV by Arrhenius fitting ($\rho = \rho_0 e^{-E_g/2k_BT}$). This is in good agreement with the Mott-Hubbard gap, that is, the intersite d-d transition between vanadium cations in inelastic neutron [21] and optical studies [22,23]. In the first stage, E_g decreases to 96 meV with increasing x and then begins to increase up to 186 meV at $x = 0.50$ [Fig. 1(d)]. For $x > 0.50$, E_g does not collapse and the samples show the higher resistivity than our measurement range. The existence of an electrical band gap indicates that $Sr_2VO_{4-x}H_x$ is a localized spin system, therefore, increase of the effective magnetic moment (μ_{eff}) should be expected with increasing x. A Curie-Weiss fit to the magnetic susceptibility data in the high-temperature region (200–300 K) (Fig. S1 [16]) gives the μ_{eff} value for each sample, as shown in Fig. 1(d). Although μ_{eff} increases from 1.3 μ_B/V for $x = 0.04$ to 1.8 μ_B/V for $x = 0.31$, μ_{eff} starts to decrease from 1.8 μ_B/V for $x = 0.31$ to 0.3 μ_B/V for $x = 0.83$. This trend coincides with the hydrogen-ordering process; i.e., as hydride ions start to order into the V-O planes, the magnetic susceptibility is largely suppressed with increasing electrical band gap. Considering that the valence state of the vanadium cation in $Sr_2VO_{4-x}H_x$ changes from V^{4+} ($3d^1$) to V^{3+} ($3d^2$) with increasing x, suppression of the magnetic susceptibility is rather unusual. As we will show below, the ground state of Sr_2VO_3H ($3d^2$) shows AFM ordering (high-spin state, $S = 1$) and there is no structural transition such as V-V dimerization (Fig. S2 [16]). Thus, the possibility of spin crossover or the formation of the spin singlet is ruled out for this magnetic suppression.

Figure 2(a) shows the magnetic susceptibility curve of Sr_2VO_3H in the high-temperature region. The curve shows magnetic suppression with a broad maximum ($T_{max} = 382\,\text{K}$) which appears to be a specific feature of a one-dimensional

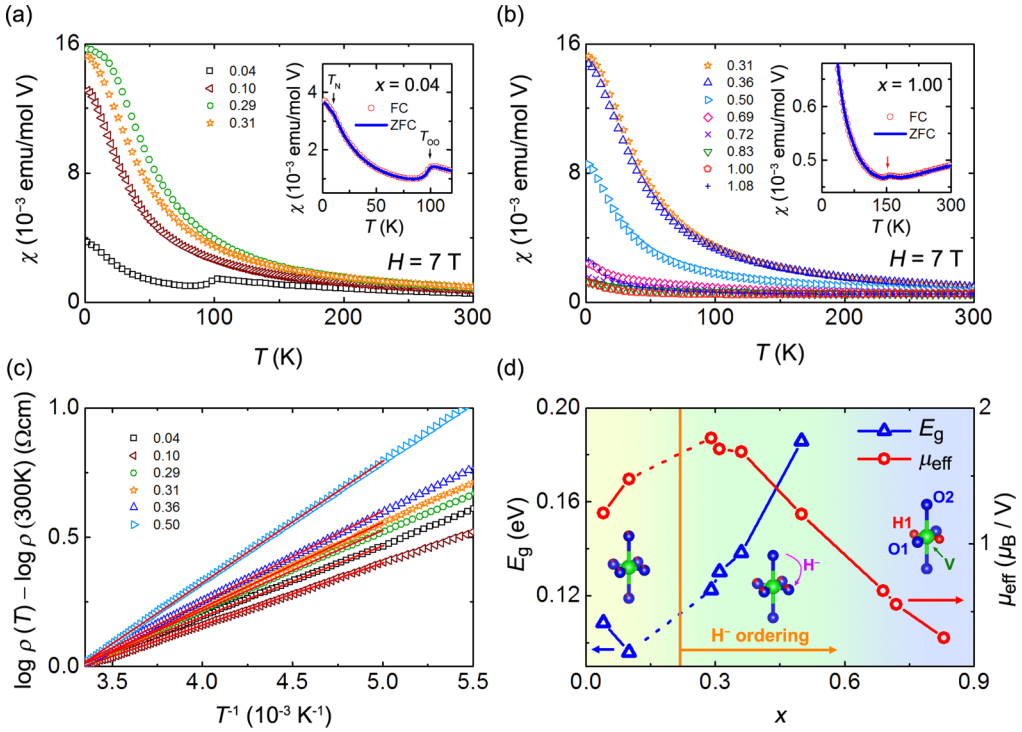

FIG. 1. (Color online) Magnetic susceptibility and electrical resistivity of polycrystalline $Sr_2VO_{4-x}H_x$ as a function of x. (a, b) Temperature-dependent magnetic susceptibility when $H = 7$ T. The inset shows the zero-field cooled (ZFC) and field cooled (FC) magnetic susceptibilities for $x = 0.04$ and 1.00. (c) Temperature-dependent electrical resistivity data and their Arrhenius fit (red line) in the range 200–300 K. For $x > 0.50$, the resistivity of each sample is beyond the range of our measurement system. (d) Electrical band gap (E_g) and effective magnetic moment (μ_{eff}) as a function of x. Hydrogen anions statistically occupy each oxygen anion site in the low hydrogen substitution region ($x < 0.25$) and are gradually ordered in the V-O plane with increasing hydrogen content, and a crystallographic transition (tetragonal to orthorhombic) occurs between $x = 0.50$ and 0.69.

antiferromagnetic spin-chain systems [11,24–36]; we will compare this data with a theoretical calculation below. As the temperature decreases, the magnetic susceptibility is gradually suppressed from 382 K and shows a large deviation from Curie-Weiss behavior. As shown in Fig. 2(c), the observed muon spin oscillation frequencies (ν) are consistent with the magnetic suppression of ~160 K in the $\chi(T)$ curve, and the magnetic moment is estimated to be 2.13 μ_B per vanadium atom, which is reasonable value for a V^{3+} ion with a $3d^2$ electron configuration. The nonmagnetic volume fraction (f_p) gradually decreases from 180 to 120 K ($\Delta T \sim 60$ K) and f_p at 2 K is only 0.14. Even though magnetic suppression appears in the $\chi(T)$ curve, no magnetic-ordering signal is present above 180 K in the μSR data, which suggests the formation of short-range AFM ordering, such as a one-dimensional Heisenberg antiferromagnet (1D-HAF) spin-chain system. The observed upturn in the low-temperature region, which is common for quasi-1D magnetic systems [11,30–32,35,37,38] possibly originates from the Curie-Weiss contribution arising from finite-length chains and/or paramagnetic impurities.

The $\chi(T)$ curve above T_N was fitted using the $S = 1$ 1D-HAF spin-chain model with the following equation [26,27]:

$$\chi_{spin} = \frac{Ng^2\mu_B^2}{k_B T}\left[\frac{2 + 0.0194x + 0.777x^2}{3 + 4.346x + 3.232x^2 + 5.834x^3}\right], \quad (1)$$

where $x = |J|/k_B T$, and $g = 2.00$. To fit the susceptibility data, we assume that the observed susceptibility consists of three terms [30,31]:

$$\chi(T) = \chi_0 + (1 - f)(\chi_{spin}) + f(\chi_{CW}), \quad (2)$$

where χ_0 is the temperature-independent term including the diamagnetic contribution of the ion core, χ_{spin} is the spin contribution of the V^{3+} ions, and χ_{CW} is a Curie-Weiss component arising from finite-length chains and/or paramagnetic impurities. The experimental curve fits well (standard deviation $\chi^2 = 2.376 \times 10^{-13}$) to the 1D-HAF model (red dashed line), with $\chi_0 = -3.316 \times 10^{-4}$ emu/mol V and exchange coupling constant $J = -29.1$ meV ($|J|/k_B = 338$ K, $|J|/T_{max} \sim 0.88$). The contribution of the Curie-Weiss component is 3.4% ($f = 0.034$) and the Curie-Weiss temperature $\theta = -18$ K. Assuming that the origin of the Curie-Weiss contribution is the paramagnetic impurity phase containing V^{3+} or V^{4+} ions, the secondary phase corresponding to 3.4 or 9.1 mol % of the total V ions should be detected by neutron diffraction measurement. However, such a significant amount of magnetic impurities was not observed in the Sr_2VO_3H sample ($Sr_2VO_3H = 93$ wt %, and SrO = 7 wt %) [6]. Therefore, the finite-length chain effect in the main phase is more likely to be the cause of the Curie-Weiss contribution [30]. Figure 2(b) shows the temperature-dependent spin susceptibility (χ_{spin}) curve of Sr_2VO_3H with the theoretical curves by $S = 1$ 1D-HAF model for various values of J. When $T > T_N$, χ_{spin}

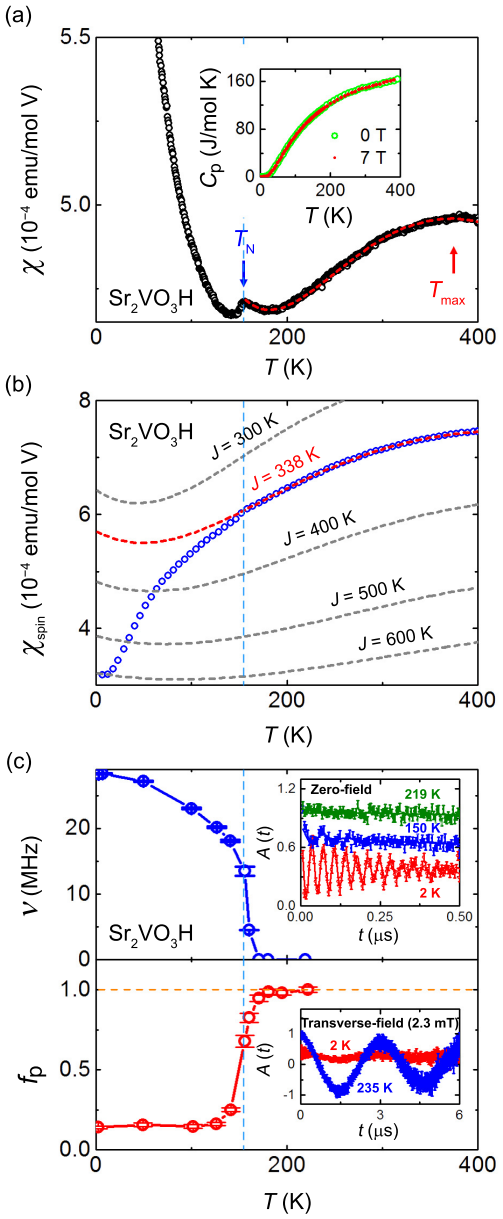

FIG. 2. (Color online) Low-dimensional behavior of Sr_2VO_3H. (a) Temperature-dependent magnetic susceptibility of Sr_2VO_3H ($x = 1.00$) in the high-temperature region. The red dashed curve shows the theoretical trace of the 1D-HAF spin-chain system including 3.4% Curie-Weiss component (χ_{CW}). The inset shows the temperature-dependent heat-capacity (C_p) data for Sr_2VO_3H with and without an external magnetic field (0 and 7 T). (b) Spin susceptibility (χ_{spin}) for Sr_2VO_3H (blue open circles) and the theoretical curves (dashed lines) of the $S = 1$ 1D-HAF spin-chain model for various exchange coupling constants J. (c) Temperature-dependent muon spin oscillation frequencies (ν) and nonmagnetic volume fraction (f_p) for Sr_2VO_3H. The inset shows zero-field and transverse-field time spectra of Sr_2VO_3H at various temperatures.

is reproduced well by the 1D-HAF model with $J = 338$ K, while significant deviation from the theoretical model was found below T_N where long-range AFM ordering develops.

The inset of Fig. 2(a) shows the temperature dependence of the heat capacity. The λ-shaped magnetic heat-capacity

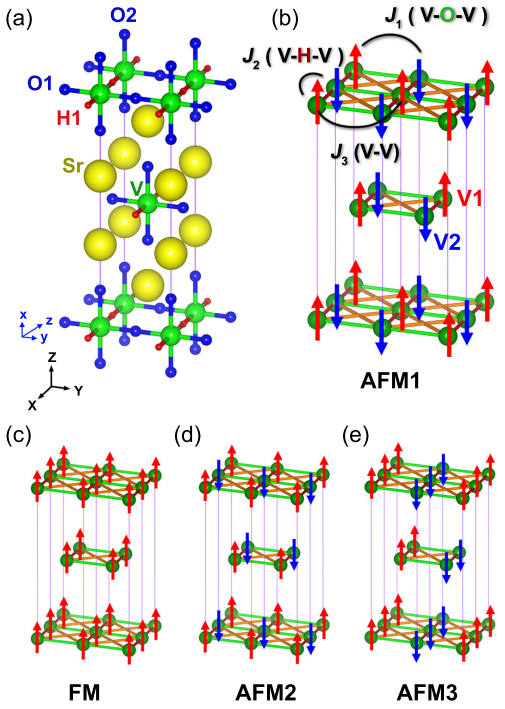

FIG. 3. (Color online) Crystal structure and ordered spin states of Sr_2VO_3H. (a) Crystal structure of the anion-ordered layered oxyhydride Sr_2VO_3H. Note that the H^- ions occupying O^{2-} sites are ordered linearly. The coordinate system for the DFT calculation is marked by blue arrows with x, y, and z. (b–e) Schematic representations of the four ordered spin states AFM1 (checkerboard), AFM2 (stripe), AFM3 (stripe), and FM of Sr_2VO_3H. J_1, J_2, and J_3 indicate the exchange coupling constants through the V-O-V, V-H-V, and V-V interaction pathways, respectively.

(C_p) peak usually associated with the paramagnetic to AFM transition is not observed with and without an external magnetic field (0 and 7 T). This heat capacity behavior is consistent with a 1D Heisenberg spin-chain system [24,39–41]; i.e., drastic entropy loss does not occur at T_N because most of the magnetic entropy above T_N is lost because of the enhanced spin fluctuation by 1D short-range magnetic ordering.

To investigate the origin of the magnetic low dimensionalization, we set the four types of spin-ordered states shown in Fig. 3 and calculated the spin-exchange coupling constants for three exchange interaction pathways using the Ising spin Hamiltonian:

$$\hat{H} = -\sum_{i<j} J_{ij} \hat{S}_{iz} \hat{S}_{jz}, \tag{3}$$

where J_{ij} is the spin-exchange coupling parameter between spin sites i and j, and $\hat{S}_{iz}$ and $\hat{S}_{jz}$ are the operators for the z components of the spin angular momentum at spin sites i and j, respectively. The total energy differences between these spin-ordered states for various on-site Hubbard interactions U (1.5–4.5 eV) and the resultant exchange coupling constants J are summarized in Table I. For each U, the AFM1 model gave the lowest total energy, which is in agreement with the experimental observations. Another important result is that the

TABLE I. Relative total energies ΔE (meV/unit cell) of the FM, AFM1, AFM2, and AFM3 spin models and exchange coupling constants J (meV) for various values of U (eV).

U	FM	AFM1	AFM2	AFM3	J_1	J_2	J_3	J_1/J_2
1.5	0	−299.46	−30.11	−252.93	−65.29	−9.58	1.03	6.82
2.5	0	−255.79	−34.84	−217.30	−54.78	−9.17	0.23	5.98
3.5	0	−216.85	−28.33	−184.50	−46.63	−7.59	0.25	6.15
4.5	0	−185.54	−23.23	−158.13	−40.05	−6.33	0.26	6.33

total energy difference between the AFM1 and AFM3 models is quite small, while the total energy of the AFM2 model is much higher than that of the AFM3 model, and it is similar to the total energy of the FM model. These results indicate that the AFM spin configuration along the V-O-V direction is energetically more stable than the FM spin configuration regardless of the spin configuration along the V-H-V direction; i.e., the formation of a 1D AFM spin chain along V-O-V is energetically stable while the interchain exchange interaction is not dominant in determining the magnetic stability. Both the V-O-V (J_1) and V-H-V (J_2) exchange interactions show antiferromagnetic interactions (negative J), and there is a large anisotropy between the two exchange energies, with a J_1/J_2 ratio of ∼6 for the different values of U. These results indicate that the antiferromagnetic superexchange interaction between vanadium cations through the oxide ion is much stronger than that through the hydride ion. Although the interatomic distance between vanadium cations in V-H-V (3.68 Å) is shorter than that in V-O-V (3.89 Å), the value of J_1 is six times larger, indicating that the superexchange interaction strongly relies on the identity of the intervening anion, not the spatial distance, in the present case.

As mentioned earlier, the symmetric relationship between magnetic ions and bridging anions plays a key role in the superexchange interaction between magnetic ions. The hydride ion has only a spherical 1s orbital, which is strikingly different from an oxide ion, which has energetically available 2p orbitals with an anisotropic shape. This different orbital nature causes different symmetric relationships with vanadium cations. Table II shows the hopping integrals between V 3d and O 2p, and V 3d and H 1s orbitals using MLWFs based on the results of a GGA + U calculation (Figs. S3 and S4 [16]). For an oxide ion in the V-O planes [O1; see the crystal structure in Fig. 3(a)], hopping is dominant between V d_{xy} and O p_x, V d_{yz} and O p_z, and V $d_{x^2-y^2}$ and O p_y orbitals, which form d-p π- and d-p σ-exchange interactions. In contrast, for a hydride ion, hopping between H s and V d_{z^2} orbitals is dominant, which gives rise to only the d-s σ-exchange interaction. The hopping integral of d-s σ bonding for a hydride ion is 2.2 eV, which is larger than that of the d-p σ bonding for an oxide ion (1.7–1.8 eV), and d-p π bonding for an oxide ion has the smallest value of ∼1 eV. This result is reasonable because the exchange interaction of σ bonding is stronger than that of π bonding and the interatomic distance between V and H is shorter than that of V and O. Considering the stronger hopping integral between H 1s and V 3d orbitals than between O 2p and V 3d orbitals, the superexchange interaction along the V-H-V direction seems to be stronger than that along the V-O-V direction, which is the opposite conclusion from the calculated exchange interaction. However, the orbital occupancy should be considered because the exchange interaction strongly depends on the occupancy of the interacting orbitals.

Figures 4(a)–4(d) show the total and partial density of states (DOSs) for Sr_2VO_3H. The partial density of states (PDOSs) show the energy overlap of relevant orbitals that participate in π- and σ-exchange interactions, which is consistent with the results of the hopping integrals in Table II. By calculating the spin occupancy for each V d orbital, we found that most unpaired spins are occupied in the V d_{xz} (48.1%) and d_{yz} (45.4%) orbitals, and only a small portion are distributed in the V d_{z^2} (2.5%) and V $d_{x^2-y^2}$ (1.9%) orbitals as shown in Table II. This finding means that most unpaired spins are associated with the π-exchange interaction with the oxide ion along the V-O-V chain direction, and only a small portion of unpaired spins participate in the σ-exchange interaction with oxide and hydride ions. Therefore, anisotropic superexchange interactions are formed and a 1D AFM spin chain developed along the V-O-V direction despite the larger σ-hopping strength between V and H because the spherical s orbital of the hydride ion is orthogonal to the V d_{xy}, d_{yz}, and d_{xz} orbitals, as shown in Figs. 4(e) and 4(f). These results suggest an alternative approach for tuning the physical dimensionality using heteromorphic mixed anions which is totally different from the conventional route, that is, control of the orbital overlap between neighboring ions.

TABLE II. Hopping integrals (eV) between V 3d and O 2p, and V 3d and H 1s orbitals in Sr_2VO_3H (spin up/down) and the number of unpaired spins for each V 3d orbital [Occ.(%)].

	O1 p_x	O1 p_y	O1 p_z	O2 p_x	O2 p_y	O2 p_z	H1 s	Occ.
V1 d_{xy}	1.15/1.18	0.00/0.00	0.00/0.00	0.00/0.00	1.02/1.02	0.00/0.00	0.00/0.00	2.1
V1 d_{xz}	0.00/0.00	0.00/0.00	0.00/0.00	0.00/0.00	0.00/0.00	1.04/1.21	0.00/0.00	48.1
V1 d_{yz}	0.00/0.00	0.00/0.00	1.17/1.34	0.00/0.00	0.00/0.00	0.00/0.00	0.00/0.00	45.4
V1 $d_{x^2-y^2}$	0.00/0.00	1.82/1.82	0.00/0.00	1.69/1.70	0.00/0.00	0.00/0.00	0.06/0.06	1.9
V1 d_{z^2}	0.00/0.00	0.69/0.78	0.00/0.00	0.58/0.67	0.00/0.00	0.00/0.00	2.20/2.15	2.5

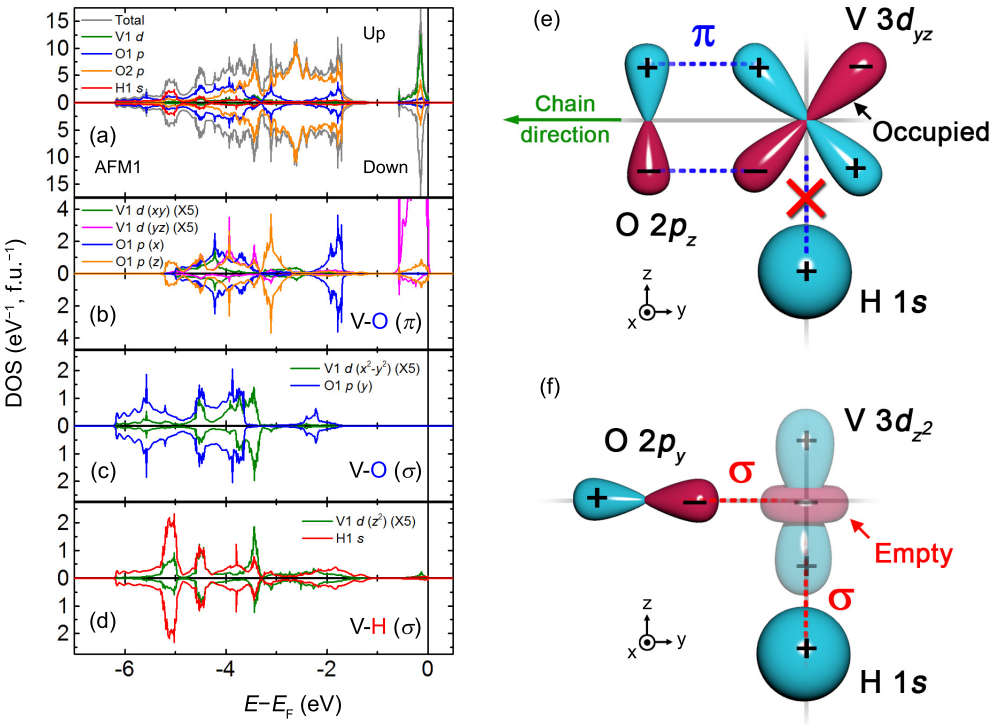

FIG. 4. (Color online) Calculated electronic structure of Sr_2VO_3H. (a–d) Total DOS and atomic PDOSs for the AFM1 model using MLWFs based on the results of a GGA + U calculation with $U = 3.5$ eV. The total DOS is the sum of the PDOSs of V, O, and H (excluding Sr). The direction along the V-H bond is set to the z axis. (e, f) Schematic diagram of the orbital interaction to explain magnetic low dimensionalization by hydride ion substitution. Hydride ion substitution breaks the π-exchange interaction between the *TM* and an oxide ion.

IV. SUMMARY

We reported low dimensionalization of magnetic ordering in *TM* oxides driven by change in the valence orbital symmetry of a bridging anion. Formation of a quasi-1D AFM spin chain occurred through the second-nearest neighbor of the vanadium cation with hydrogen ordering in $Sr_2VO_{4-x}H_x$ with $x \sim 1$. Substitution of a hydride ion for an oxide ion can break the π-exchange interaction between the *TM* ion and the oxide ion, causing an anisotropic exchange interaction. In the case of early *TM* oxides in which only the d_{xy}, d_{yz}, and d_{xz} orbitals are occupied, the absence of an exchange pathway through *TM*-H-*TM* can introduce low dimensionalization in the three-dimensional crystal structure when the substituted hydride ions are ordered low dimensionally. For *TM* oxides with electrons occupying the $d_{x^2-y^2}$ and d_{z^2} orbitals, the σ-exchange interaction through *TM*-H-*TM* works effectively, so the low-dimensionalization effect described above is negligible. Thus, we may understand the strong AFM ordering ($T_N > 350$ K) [1] reported for Co-based oxyhydrides by the high occupation of unpaired spins in $d_{x^2-y^2}$ and d_{z^2} orbitals, which forms the strong superexchange interaction through the Co-H-Co pathway in addition to the Co-O-Co pathway. The present finding indicates the possibility achieving unique electronic and magnetic behavior of *TM* compounds by utilizing heteromorphic mixed anions.

ACKNOWLEDGMENTS

We acknowledge Dr. H. Mizoguchi, Dr. H. Lei, Dr. K. Lee, Dr. Y. Muraba, Dr. S. Jeong, Dr. M. Miyazaki, Dr. H. Okabe, Dr. A. Koda, and Dr. R. Kadono for discussions. This study was supported by MEXT, Element Strategy Initiative to form a research core.

[1] M. A. Hayward, E. J. Cussen, J. B. Claridge, M. Bieringer, M. J. Rosseinsky, C. J. Kiely, S. J. Blundell, I. M. Marshall, and F. L. Pratt, Science **295**, 1882 (2002).
[2] K. Poeppelmeier, Science **295**, 1849 (2002).
[3] R. M. Helps, N. H. Rees, and M. A. Hayward, Inorg. Chem. **49**, 11062 (2010).
[4] Y. Kobayashi, O. J. Hernandez, T. Sakaguchi, T. Yajima, T. Roisnel, Y. Tsujimoto, M. Morita, Y. Noda, Y. Mogami, A. Kitada, M. Ohkura, S. Hosokawa, Z. Li, K. Hayashi, Y. Kusano, J. Kim, N. Tsuji, A. Fujiwara, Y. Matsushita, K. Yoshimura *et al.*, Nat. Mater. **11**, 507 (2012).
[5] T. Sakaguchi, Y. Kobayashi, T. Yajima, M. Ohkura, C. Tassel, F. Takeiri, S. Mitsuoka, H. Ohkubo, T. Yamamoto, J. Kim, N. Tsuji, A. Fujihara, Y. Matsushita, J. Hester, M. Avdeev, K. Ohoyama, and H. Kageyama, Inorg. Chem. **51**, 11371 (2012).
[6] J. Bang, S. Matsuishi, H. Hiraka, F. Fujisaki, T. Otomo, S. Maki, J.-I. Yamaura, R. Kumai, Y. Murakami, and H. Hosono, J. Am. Chem. Soc. **136**, 7221 (2014).

[7] F. Denis Romero, A. Leach, J. S. Möller, F. Foronda, S. J. Blundell, and M. A. Hayward, Angew. Chem. **126**, 7686 (2014).
[8] J. Kanamori, J. Phys. Chem. Solids **10**, 87 (1959).
[9] M. T. Hutchings, G. Shirane, R. J. Birgeneau, and S. L. Holt, Phys. Rev. B **5**, 1999 (1972).
[10] I. U. Heilmann, G. Shirane, Y. Endoh, R. J. Birgeneau, and S. L. Holt, Phys. Rev. B **18**, 3530 (1978).
[11] W. E. Estes, D. P. Gavel, W. E. Hatfield, and D. J. Hodgson, Inorg. Chem. **17**, 1415 (1978).
[12] R. M. Morra, W. J. L. Buyers, R. L. Armstrong, and K. Hirakawa, Phys. Rev. B **38**, 543 (1988).
[13] P. Blaha, K. Schwarz, G. K. H. Madsen, D. Kvasnicka, and J. Luitz, WIEN2K, *An Augmented Plane Wave + Local Orbitals Program for Calculating Crystal Properties* (Karlheinz Schwarz, Technische Universität Wien, Austria, 2001).
[14] K. Schwarz, J. Solid State Chem. **176**, 319 (2003).
[15] J. P. Perdew, K. Burke, and M. Ernzerhof, Phys. Rev. Lett. **77**, 3865 (1996).
[16] See Supplemental Material at http://link.aps.org/supplemental/10.1103/PhysRevB.92.064414 for additional details on the magnetic properties, lattice parameters, and first-principle calculations.
[17] A. A. Mostofi, J. R. Yates, Y.-S. Lee, I. Souza, D. Vanderbilt, and N. Marzari, Comput. Phys. Commun. **178**, 685 (2008).
[18] J. Kuneš, R. Arita, P. Wissgott, A. Toschi, H. Ikeda, and K. Held, Comput. Phys. Commun. **181**, 1888 (2010).
[19] H. D. Zhou, B. S. Conner, L. Balicas, and C. R. Wiebe, Phys. Rev. Lett. **99**, 136403 (2007).
[20] J. Sugiyama, H. Nozaki, I. Umegaki, W. Higemoto, E. J. Ansaldo, J. H. Brewer, H. Sakurai, T.-H. Kao, H.-D. Yang, and M. Månsson, Phys. Rev. B **89**, 020402 (2014).
[21] H. D. Zhou, Y. J. Jo, J. Fiore Carpino, G. J. Munoz, C. R. Wiebe, J. G. Cheng, F. Rivadulla, and D. T. Adroja, Phys. Rev. B **81**, 212401 (2010).
[22] J. Matsuno, Y. Okimoto, M. Kawasaki, and Y. Tokura, Phys. Rev. Lett. **95**, 176404 (2005).
[23] J. Matsuno, Y. Okimoto, M. Kawasaki, and Y. Tokura, Appl. Phys. Lett. **82**, 194 (2003).
[24] J. C. Bonner and M. E. Fisher, Phys. Rev. **135**, A640 (1964).
[25] W. E. Estes, R. R. Weller, and W. E. Hatfield, Inorg. Chem. **19**, 26 (1980).
[26] A. Meyer, A. Gleizes, J. J. Girerd, M. Verdaguer, and O. Kahn, Inorg. Chem. **21**, 1729 (1982).
[27] V. Gadet, M. Verdaguer, V. Briois, A. Gleizes, J. P. Renard, P. Beauvillain, C. Chappert, T. Goto, K. Le Dang, and P. Veillet, Phys. Rev. B **44**, 705 (1991).
[28] M. Hase, I. Terasaki, and K. Uchinokura, Phys. Rev. Lett. **70**, 3651 (1993).
[29] S. Eggert, I. Affleck, and M. Takahashi, Phys. Rev. Lett. **73**, 332 (1994).
[30] T. Ami, M. K. Crawford, R. L. Harlow, Z. R. Wang, D. C. Johnston, Q. Huang, and R. W. Erwin, Phys. Rev. B **51**, 5994 (1995).
[31] N. Motoyama, H. Eisaki, and S. Uchida, Phys. Rev. Lett. **76**, 3212 (1996).
[32] J. L. Dye, Inorg. Chem. **36**, 3816 (1997).
[33] R. H. Huang, M. J. Wagner, D. J. Gilbert, K. A. Reidy-Cedergren, D. L. Ward, M. K. Faber, and J. L. Dye, J. Am. Chem. Soc. **119**, 3765 (1997).
[34] K. Fabricius, A. Klümper, U. Löw, B. Büchner, T. Lorenz, G. Dhalenne, and A. Revcolevschi, Phys. Rev. B **57**, 1102 (1998).
[35] T. Masuda, T. Sakaguchi, and K. Uchinokura, J. Phys. Soc. Jpn. **71**, 2637 (2002).
[36] H. H. Ko, J. H. Lim, H. C. Kim, and C. S. Hong, Inorg. Chem. **45**, 8847 (2006).
[37] E. E. Kaul, H. Rosner, V. Yushankhai, J. Sichelschmidt, R. V. Shpanchenko, and C. Geibel, Phys. Rev. B **67**, 174417 (2003).
[38] M. D. Johannes, J. Richter, S.-L. Drechsler, and H. Rosner, Phys. Rev. B **74**, 174435 (2006).
[39] L. J. De Jongh and A. R. Miedema, Adv. Phys. **50**, 947 (2010).
[40] M. D. Chabot and J. T. Markert, Phys. Rev. Lett. **86**, 163 (2001).
[41] K. Kudo, S. Kurogi, Y. Koike, T. Nishizaki, and N. Kobayashi, Phys. Rev. B **71**, 104413 (2005).